

Observations of relativistic plasma waves excited by a 1.064 μm and 1.053 μm laser beat

A Dyson[†], A E Dangor[†], A K L Dymoke-Bradshaw[†], T Ashfar-Rad[†],
P Gibbon[†], A R Bell[†], C N Danson[‡], C B Edwards[‡], F Amiranoff[§],
G Matthieusent^{||}, S J Karttunen[¶] and R R E Salomaa[¶]

[†] Imperial College of Science and Technology and Medicine, London SW7, UK

[‡] Rutherford Appleton Laboratory, Chilton, Didcot, Oxfordshire OX11 0QX, UK

[§] Laboratoire pour L'Utilisation des Laser Intenses, Ecole Polytechnique, CNRS, 91128 Palaiseau, France

^{||} Laboratoire de Physique des Gaz et des Plasma, Univ. Paris Sud, CNRS, 91405 Orsay, France

[¶] Nuclear Engineering Laboratory, Technical Research Centre of Finland, SF-00181 Helsinki, Finland

Received 17 November 1995

Abstract. We report observations of a relativistic plasma wave excited by two copropagating laser beams with frequency difference close to the plasma frequency in a fully ionized hydrogen plasma. The laser beams were at 1.064 μm (Nd:YAG) and 1.053 μm (Nd:YLF) of 200 ps duration and focused to a $\approx 7\times$ diffraction limit spot with peak irradiance of $2 \times 10^{14} \text{ W cm}^{-2}$. The plasma wave was detected by monitoring the forward-scattered spectrum of a third copropagating laser beam at 0.526 μm . A novel use of Moire deflectometry ensured the pump beams and probe beam were copropagating at focus. The inferred plasma wave density modulation $\delta n/n$ is about 1–2% and corresponds to a longitudinal electric field of about 10^9 V m^{-1} . The plasma wave was observed to exist for a time $\tau_p \leq 50 \text{ ps}$. These results are not in agreement with theoretical predictions for relativistic detuning which give $\delta n/n \approx 8\%$, $\tau_p \approx 200 \text{ ps}$ and suggest that there is some mechanism limiting the growth of the plasma wave. Simulations indicate that this is due to either ponderomotive blowoff taking the plasma off resonant density or to the modulational instability.

1. Introduction

Considerable interest has been shown in the use of lasers to generate large amplitude plasma waves by the beat wave process (Tajima and Dawson 1979, Cohen *et al* 1972). In the beat wave two laser beams with slightly different frequencies ω_0, \mathbf{k}_0 and ω_1, \mathbf{k}_1 beat together to generate a plasma wave at the difference frequency $\Delta\omega = \omega_1 - \omega_0$ with wavevector $\Delta\mathbf{k} = \mathbf{k}_1 - \mathbf{k}_0$. Very large amplitude plasma waves can be generated if the beat frequency $\Delta\omega$ is close to the plasma frequency ω_p , the resonant frequency for plasma wave excitation. The plasma wave amplitude is ultimately limited by relativistic detuning where the oscillation of plasma electrons in the combined fields of the laser and plasma wave results in a decrease in the plasma frequency taking the system off resonance. The phase velocity of the plasma wave is $v_p = \Delta\omega/|\Delta\mathbf{k}|$ and has an associated relativistic factor $\gamma = (1 - v_p^2/c^2)^{1/2}$. This limits the maximum energy that an injected electron can gain as $\Delta W \propto \gamma^2(\delta n/n)$ where $\delta n/n$ is the wave amplitude. If the plasma is very underdense with $\omega_p \ll \omega_{0,1}$ then for copropagating laser beams the plasma wave has phase velocity

close to c with $\gamma \approx \omega_{0,1}/\omega_p \gg 1$. Thus, the longitudinal electric field associated with a large amplitude plasma wave can be used to accelerate electrons to relativistic energies over distances of metres rather than the tens of kilometres needed using conventional technology. Large amplitude plasma waves have other applications such as plasma diagnostics, plasma heating and current drive (Cohen *et al* 1972, 1988, Karttunen *et al* 1991).

Plasma wave generation by the beat wave mechanism has been demonstrated with microwaves (Rogers *et al* 1992), CO₂ laser beams (Clayton *et al* 1985, 1993, Ebrahim *et al* 1986, Ebrahim 1994, Kitagawa *et al* 1992) and neodymium glass laser beams (Dangor *et al* 1990, Amiranoff *et al* 1992, 1995). Rogers *et al* (1992) used two microwave beams tunable to wavelengths in the range 3–3.5 cm. Their experiment differs from the others mentioned above in that the two beams were counterpropagating and so gave very low phase velocity plasma waves with $\gamma \approx 1$. Clayton *et al* (1985) used a CO₂ laser at 9.6 μm and 10.6 μm to obtain a plasma wave of amplitude $\delta n/n \approx 1\text{--}3\%$ with $\gamma \approx 10$. A somewhat larger plasma wave was reported by Ebrahim *et al* (1986) using the same laser wavelengths. In a more recent experiment, Clayton *et al* (1993) used laser beams at 10.3 μm and 10.6 μm to give a plasma wave with $\gamma \approx 30$ and observed that electrons injected at ≈ 2 MeV were accelerated to energies > 10 MeV, the limit of the detection system. The inferred plasma wave amplitude $\delta n/n$ was greater than 10% and corresponds to a longitudinal electric field greater than 10^9 V m⁻¹. This should be compared with the value of 10^5 V m⁻¹ in current particle accelerators. Kitagawa *et al* (1992) performed similar experiments using a CO₂ laser but without injecting electrons. They reported the presence of plasma electrons accelerated to energies > 10 MeV, which implied the existence of a plasma wave with $\delta n/n \approx 5\%$. The latest experiment by Ebrahim (1994) has shown acceleration of 12.5 MeV electrons up to energies of 28 MeV by a plasma wave with $\delta n/n \approx 17\%$.

Two series of experiments using glass lasers, both operating at 1.064 μm (Nd:YAG) and 1.053 μm (Nd:YLF) have been reported (Dangor *et al* 1989, Amiranoff *et al* 1992, 1995). Here, the plasma wave has $\gamma \approx 100$ and so allows acceleration to much higher energies. However, in these experiments the plasma electron density has to be set to $< 0.5\%$ of the exact resonant density compared with the much less stringent requirement of $< 5\%$ for CO₂ lasers (Karttunen and Salomaa 1989). This difficulty was overcome by using laser ionization of hydrogen gas to give a fully ionized plasma. Laser ionization is classed as either tunnel ionization or multiphoton ionization according to the Keldysh parameter $K = (E_i/2\Phi_p)^{1/2}$, where E_i is the ionization energy and $\Phi_p = m_e(v_{\text{osc}}^2)/2$ is the ponderomotive potential (Keldysh 1965). The Keldysh parameter is defined so that $K \propto (\omega\tau)^{1/2}$ where ω is the laser frequency and τ is the time taken by an electron to tunnel out of the Coulomb barrier. For $K \ll 1$ the tunnelling time is much shorter than the laser period and tunnel ionization is favoured. Another relevant parameter is the number of photons required for ionization $n_\gamma \approx E_i/h\omega$; as n_γ increases multiphoton ionization becomes increasingly difficult. In Dangor *et al* (1988) a 0.526 μm beam was found to generate a fully ionized resonant density plasma over a length of at least 10 mm. In that experiment $I = 5 \times 10^{13}$ W cm⁻² so that $\Phi_p \approx 0.2$ eV and for hydrogen ($E_i \approx 13.6$ eV) we have $K \approx 5$, $n_\gamma = 6$ giving multiphoton ionization. Similar multiphoton ionization experiments for beat wave plasmas have been reported in Marques *et al* (1993). It was found in our experiment that a green ionizer beam was not necessary as the pumps alone gave full ionization. The pumps had intensity $I \approx 2 \times 10^{14}$ W cm⁻² so that $\Phi_p \approx 19$ eV and $K \approx 0.5$, $n_\gamma = 12$ also giving multiphoton ionization. This should be compared with the CO₂ experiments for which $I \approx 3 \times 10^{14}$ W cm⁻² so that $\Phi_p \approx 3 \times 10^3$ eV and $K \approx 0.05$, $n_\gamma \approx 135$ giving tunnel ionization (Leemans *et al* 1992). The other main difficulty in using an Nd laser is that the resulting focal spot is typically several times the diffraction limit

compared with approximately equal to the diffraction limit for CO₂ lasers. This corresponds to distortion of the pump beam intensity and phase fronts in the focal region so that the plasma wave is generated over a smaller radial dimension than the full spot size. This results in stronger ponderomotive blowoff taking the system off resonance and so limits the plasma wave amplitude. In the experiment reported here (Dangor *et al* 1990) the relativistic plasma wave was observed directly by measuring the anti-Stokes sideband at ω_p generated by the interaction of the plasma wave with a copropagating 0.526 μm laser probe. The inferred plasma wave had a measured amplitude of $\delta n/n \approx 1\text{--}2\%$ corresponding to an electric field of 10^9 V m^{-1} and lifetime $\tau_p \leq 50 \text{ ps}$. Both the amplitude and duration of the sideband were shorter than expected for relativistic detuning at $\delta n/n \approx 8\%$, $\tau_p \approx 200 \text{ ps}$. In a similar experiment by Amiranoff *et al* (1992) both Stokes and anti-Stokes sidebands at multiples of the plasma frequency were observed again using a 0.526 μm copropagating laser probe. However, the sidebands were observed on light scattered at 10° and are thus due to secondary low-velocity plasma waves propagating almost at right angles to the pump beams. These secondary waves were presumed to be due to the modulational decay of a plasma wave with $\delta n/n \approx 2\%$. A recent experiment by Amiranoff *et al* (1995) has observed that electrons injected at $\approx 3 \text{ MeV}$ are accelerated to $\approx 4 \text{ MeV}$ by a relativistic plasma wave with similar amplitude.

In this paper, we present a detailed account of the experiment reported only briefly in Dangor *et al* (1990). We begin with a discussion of the basic scaling of the beat wave scheme. We then give the details of the laser configuration used to produce the pump beams and the combining of the beams on target to minimize energy loss. We present typical intensity and phase profiles in the focal region that are calculated using a diffraction code for our $\approx 7\times$ diffraction limited spot. We show that the plasma wave is generated over a radial dimension of the diffraction limit of the focusing lens. The use of the copropagating frequency-doubled probe beam for diagnosing the plasma wave is detailed. We then calculate the plasma wave amplitudes for our experimental conditions and show that the small radial dimension of the plasma wave (one seventh of the beam size) results in strong ponderomotive blowoff. This is found to limit the plasma wave amplitude and lifetime to our measured values. In addition, we give here the results of a PIC code used to model the modulational instability which would also limit the plasma wave amplitude and lifetime to our measured values.

2. Basic scaling of the beat wave process

In this section we present a simple 1D analysis where it is assumed that the laser is focused to the diffraction limit so giving planar phase fronts. The growth rate of the plasma wave is linear initially and is given by (Rosenbluth and Liu 1972)

$$\frac{d\varepsilon}{dt} = \frac{1}{4}\alpha_0\alpha_1\omega_p \quad (2.1)$$

where $\varepsilon = \delta n/n$ is the relative amplitude of the plasma wave and $\alpha_i = eE_i/m\omega_i c$ is the oscillating velocity of an electron in the laser pump fields relative to the speed of light; $\alpha_i \propto (I_i\lambda_i^2)^{1/2}$ where I_i and λ_i are the intensities and wavelengths of the laser beams. Thus, if the laser fields are step functions then the initial growth $\propto (I_0\lambda_0^2 I_1\lambda_1^2)^{1/2} = I\lambda^2$.

As the wave amplitude and oscillation velocity increase there is a relativistic increase in the electron mass and hence a decrease in the plasma frequency which results in detuning

and saturation of the wave at (Rosenbluth and Liu 1972)

$$\varepsilon_{\text{sat}} = \left[\frac{16}{3} \alpha_0 \alpha_1 \right]^{1/3}. \quad (2.2)$$

Tang *et al* (1985) have shown that a higher ε_{sat} may be obtained by a deliberate initial frequency mismatch and have calculated the amount by which ω_p has to exceed the frequency difference $\omega_1 - \omega_0$ to maximize ε_{sat} . However, this is difficult to access experimentally and thus we use the saturation limit above. Assuming the linear growth rate (2.1) is maintained, the time to reach saturation t_{sat} is given by

$$\omega_p t_{\text{sat}} \approx 4 \left(\frac{16}{3} \right)^{1/3} \left(\frac{1}{\alpha_0 \alpha_1} \right)^{2/3} \quad (2.3)$$

for constant laser fields. Thus $\varepsilon_{\text{sat}} \propto (I\lambda^2)^{1/3}$ and $t_{\text{sat}} \propto (I\lambda^2)^{-2/3}$. If the laser pulses are longer than t_{sat} the plasma wave amplitude will decrease and oscillations set in. This is because whenever the phase difference between the laser beat and the plasma wave is between $(n+1/2)\pi$ and $(n+1)\pi$ the energy transfer is reversed and is from the plasma wave to the laser fields (Karttunen and Salomaa 1986, 1987). Thus, ideally the pulse duration of the laser beams τ should be matched to the saturation time t_{sat} . Assuming this to be the case, (2.1) and (2.2) give

$$\varepsilon_{\text{sat}} = \left[\frac{64}{3} \frac{1}{\omega_p \tau} \right]^{1/2} \quad (2.4)$$

and

$$\alpha_0 \alpha_1 = \frac{32}{\sqrt{3}} \left[\frac{1}{\omega_p \tau} \right]^{3/2}. \quad (2.5)$$

These equations determine ε_{sat} and $I\lambda^2$ for the optimum case of $\tau = t_{\text{sat}}$. The energy required to drive the plasma wave is $W = I\tau(\pi\sigma^2)$ where σ is the radius of the laser beams. We thus see that ε_{sat} , $I\lambda^2$ and W vary as some inverse power of the pulse duration τ .

The plasma wave will also saturate due to linear detuning, i.e. when the plasma frequency is not resonant with the laser beat frequency. The maximum amplitude due to this is (Mora *et al* 1988)

$$\varepsilon_{\text{max}} = \alpha_0 \alpha_1 \left(\frac{\Delta n}{n} \right)^{-1} \quad (2.6)$$

where Δn is the density mismatch from resonance and is given by

$$\frac{\Delta n}{n} = 2 \frac{\omega_p - \Delta\omega}{\omega_p}. \quad (2.7)$$

The allowable mismatch from resonance is calculated by requiring the wave amplitude due to linear detuning to be less than that due to relativistic detuning. This then gives

$$\left(\frac{\Delta n}{n} \right)_{\text{max}} = \frac{4}{\omega_p \tau}. \quad (2.8)$$

The density mismatch can be larger for shorter laser pulses since $\varepsilon_{\text{sat}} \propto \tau^{-1/2}$.

Density mismatch can also occur as a result of the radial motion of the plasma due to the ponderomotive forces associated with radial gradients of the pump beams and plasma wave (Mora *et al* 1988). The force on an ion due to the ponderomotive force is

$$m_i \frac{dv_r}{dt} = -\nabla_r \frac{1}{4} m_e v_{\text{osc}}^2 \quad (2.9)$$

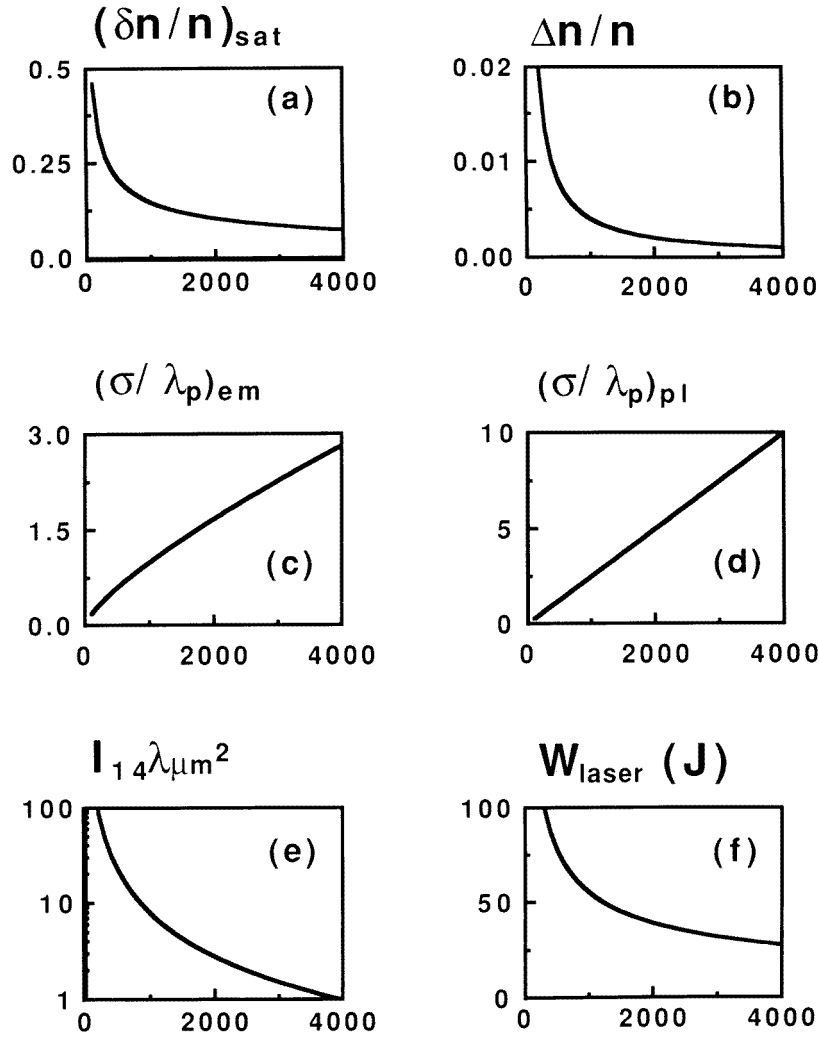


Figure 1. The beat wave scaling with the pulse duration τ matched to the saturation time t_{sat} . In all graphs the abscissa is $\omega_p \tau$. (a) Plasma wave amplitude $(\delta n/n)_{\text{sat}}$ due to relativistic detuning; (b) the maximum allowable density mismatch $\Delta n/n$; (c) and (d) the minimum beam radius σ/λ_p imposed by the ponderomotive force due to the laser pumps and plasma waves, respectively; (e) and (f) the laser intensity and energy required to drive the plasma wave to saturation. I_{14} is the intensity in units of $10^{14} \text{ W cm}^{-2}$ and $\lambda_{\mu\text{m}}$ is the laser wavelength in μm . The laser energy $W_{\text{laser}}(\text{J})$ is calculated for a plasma density $n_e = 10^{17} \text{ cm}^{-3}$, laser spot radius $\sigma = 2\lambda_p$ and plasma wave $\gamma = 100$ as in our experiment.

where v_{osc} is the oscillation velocity of an electron in the combined electric fields of the laser beams and the plasma wave. Using the requirement that the density mismatch due to this motion saturates the plasma wave at a value less than ε_{sat} , (2.2), (2.5) and (2.8) give the minimum beam radius. For Gaussian profiles $I \propto \exp(-r^2/\sigma^2)$, the ponderomotive force due to the laser beams gives

$$\frac{\omega_p \sigma_{\text{min}}}{c} = \left(\frac{m_e}{m_i} \right)^{1/2} \frac{2}{3^{1/4}} (\omega_p \tau)^{3/4} \quad (2.10)$$

and that for the plasma wave gives

$$\frac{\omega_p \sigma_{\min}}{c} = \left(\frac{m_e}{m_i} \right)^{1/2} \frac{2}{3} (\omega_p \tau). \quad (2.11)$$

These results are consistent within a small numerical factor with the saturation amplitudes given by Mora *et al* (1988).

Figure 1 depicts the scaling results given above as functions of $\omega_p \tau$. Figure 1(a) illustrates the fact that a shorter laser pulse is required to drive the plasma wave to a higher relativistic saturation limit. Figure 1(b) shows that a much larger density mismatch can be tolerated when a shorter laser pulse is used. This is the real advantage of generating larger amplitude plasma waves using higher intensity, shorter laser pulses. The other advantage is that the lasers can then be focused to a smaller beam size before ponderomotive blowoff is important, as shown in figures 1(c) and 1(d). The plasma wave ponderomotive force imposes the strictest condition on beam size. Note that the beam radius cannot be reduced to less than c/ω_p to avoid nonlinearities associated with plasma wave magnetic fields which would give a lower saturation value (Bell and Gibbon 1988). Figure 1(e) shows that greater laser intensity is required for each beam when using shorter laser pulses. The laser energy required in each beam is $W_{\text{laser}} \propto n_e^{3/2} \sigma^2 \gamma^2$ and is plotted in figure 1(f) for our wavelengths, assuming $\sigma = 200 \mu\text{m}$.

In our experiment $\lambda_0 = 1.064 \mu\text{m}$ and $\lambda_1 = 1.053 \mu\text{m}$; thus,

$$\begin{aligned} \omega_p &= 1.85 \times 10^{13} \text{ s}^{-1} & \lambda_p &= 2\pi c/\omega_p = 100 \mu\text{m} \\ n_e &= 1.08 \times 10^{17} \text{ cm}^{-3} & \gamma &= \sqrt{\omega_0 \omega_1} / \omega_p = 97. \end{aligned} \quad (2.12)$$

The pulse duration was 200 ps fwhm corresponding to $\omega_p \tau \approx 3700$, with $\sigma = 200 \mu\text{m}$. Thus, we could expect a maximum plasma wave amplitude of $(\delta n/n)_{\text{sat}} \approx 8\%$ due to relativistic detuning (see figure 1(a)). The maximum tolerable density mismatch is 0.1% (see figure 1(b)). This is an extremely stringent requirement on the reproducibility and spatial uniformity of the plasma. The minimum laser intensity and energy in each beam required to excite this plasma wave are $10^{14} \text{ W cm}^{-2}$ and 25 J (see figures 1(e) and 1(f)).

The results of the next section will show that a more realistic value for the spot size is $\sigma = 25 \mu\text{m}$ and so it is clear that the ponderomotive blowoff will significantly lower the plasma wave amplitude from the above value (see figures 1(c) and 1(d)).

3. The laser and input optics

The experiment was performed at the Rutherford Appleton Laboratory using the VULCAN laser system (Danson 1990). The two wavelengths were generated using Nd:YAG (1.064 μm) and Nd:YLF (1.053 μm) laser media. Initially, a single oscillator cavity housed both laser rods but due to poor reproducibility this was replaced by a system with separate oscillators. The outputs were then combined and fed through a common amplifier chain consisting of silicate and phosphate glass to balance the overall gain at the two wavelengths. This gave a final beam diameter of 100 mm with an output power of 0.5 TW. However, due to SRS in atmospheric nitrogen (Dangor *et al* 1989) and CARS (phonon scattering) in the amplifier medium and the optics (Dyson *et al* 1989) very strong sidebands at multiples of the difference frequency were generated. This prevented direct detection of a plasma wave by observing the much smaller amplitude sidebands formed on the pumps from interaction with the plasma wave. For this reason, separate amplifier chains were then used with the pump beams orthogonally polarized. The beams were finally made copropagating under vacuum in a mixing box situated at the entrance to the target chamber. However, despite

the above, the sidebands on the pumps could not be eliminated to an acceptable level due to CARS in quartz in the remaining common path of the pump beams. Thus, a separate copropagating $0.526\ \mu\text{m}$ green probe beam had to be used to diagnose the plasma wave. In addition, the coincidence of the probe and the pumps in the optics had to be minimized as CARS in quartz can result in sidebands on the probe again at a level greater than for a plasma wave.

A suitable plasma for the beat wave was generated by multiphoton ionization of hydrogen gas in the target chamber. As ionization is considerably easier at shorter wavelengths an intense $0.526\ \mu\text{m}$ green beam was made available for this purpose. Plasma deflectometry measurements to check the alignment of the pump beams were performed with a low-power Nd:YAG beam which was Raman shifted for wavelength discrimination from the other beams.

3.1. Laser configuration

The two oscillators were based on the design of Kuizenga and Siegman (1970). They were actively modelocked and Q-switched. A common RF drive was used for the modelocking to ensure a fixed time delay between the pulses. The synchronization of the output pulses was achieved by finely adjusting the relative output phases of the RF drive. Two separate amplifier chains were then used to amplify the pulses to the required energy. Each chain consisted of a series of rod amplifiers up to a beam diameter of 76 mm. Self-oscillation and back reflection into the oscillators were prevented using Pockels cells and Faraday isolators. The final output amplifiers were of a disc design with a clear aperture of 108 mm. These maintained beam uniformity giving larger beam diameters. Since separate amplifier chains were used it was no longer necessary to balance the pulse energies using different amplifier media. Therefore, phosphate glass amplifiers were used throughout giving a system output of about 0.5 TW. The gain at the Nd:YAG wavelength is smaller and extra amplification was necessary at this wavelength. Good beam quality was ensured by using vacuum spatial filters (VSFs) at various points in the amplifier chains. Two extra beams at the Nd:YLF wavelength were frequency doubled to give the ionizing and probe beams. A further low-energy Nd:YAG beam was Raman shifted for interferometric measurements.

3.2. Beam characterization

Good beam quality is essential in this experiment as the beat wave is essentially generated by the beating together of the phase fronts of each pump beam. The following beam characteristics were measured: pulse width, relative timing, spatial and temporal coherence and transverse uniformity.

The pulse width and beam timing for each shot were monitored using fast optical streak cameras giving 20 ps temporal resolution. This was done both in the laser chain with fibre optic pickups collecting reflected light from various components and also in the target area by imaging the final focus. In this way, the relative timing of the two pumps, the ionizer and the probe could be accurately varied, ensuring the coincidence of the pumps and probe.

The coherence length was measured using a specially constructed Fizeau interferometer in which the retro-mirror was replaced by a diffraction grating. This resulted in different parts of the beam having different time delays. Fringes were observed through the whole pulse length indicating that the coherence length is approximately the pulse duration.

The spatial uniformity of the phase fronts was estimated from the beam size at focus relative to the diffraction limit. The final vacuum spatial filters had $F = 4\ \text{m}$ focal length

lenses with 400 μm radius pinholes restricting the output beam divergence to less than 100 μrad . The measured spot size of less than 200 μm with an $F = 2$ m focusing lens corresponds to a spot size of $\approx 7\times$ the diffraction limit.

The intensity and phase fronts in the focal region were modelled with a Fresnel diffraction code. For paraxial rays the wave amplitude in the focal region $u(x, y, z)$ is related to the wave amplitude at the focusing lens $u(x_0, y_0, z_0)$ by

$$u(x, y, z) \approx \frac{i}{L\lambda} \iint u(x_0, y_0, z_0) \exp\{ik((x-x_0)^2 + (y-y_0)^2)/2L\} dx_0 dy_0 \quad (3.1)$$

where $L = z - z_0 \approx F$. The electric field is given by

$$E(x, y, z) = \text{Re}\{u(x, y, z)e^{i(kz - \omega t)}\}. \quad (3.2)$$

The lens introduces a quadratic chirp $= -ik(x_0^2 + y_0^2)/2F$ to the incident laser beam $u_0(x_0, y_0, z_0) = A \exp(i\theta)$ where A is the amplitude and θ the phase variation across the beam. The amplitude and phase were taken as constant in each computational cell. The resulting wave amplitude in the focal region is

$$u(x, y, z) = \sum_{ij} A_{ij} e^{i\theta_{ij}} \int_i \exp\{ik(x_0 x/F - x_0^2 d/2F^2)\} dx_0 \\ \times \int_j \exp\{ik(y_0 y/F - y_0^2 d/2F^2)\} dy_0. \quad (3.3)$$

The integrations were performed using standard tables of Fresnel integrals. This method is computationally much faster than the use of Fourier transforms as in Biancalana and Chessa (1994). The code was tested using standard Hermite–Gaussian modes $u_{mn}(x, y, z) = u_m(x, z)u_n(y, z)$ with

$$u_n(x, z') = \left(\frac{2}{\pi}\right)^{1/4} \left(\frac{\exp\{i(2n+1)\Psi(z')\}}{2^n n! w(z')}\right)^{1/2} H_n\left(\frac{\sqrt{2}x}{w(z')}\right) \exp\left\{i\frac{kx^2}{2R(z')} - \frac{x^2}{w^2(z')}\right\} \quad (3.4)$$

where $z' = z - F$ is measured from the best focus, $\Psi(z')$ is the Guoy phase shift ($= \pi/2$ at the lens), $w(z')$ is the Gaussian beam width and $R(z')$ the beam radius of curvature ($= F$ at the lens). It is found that the Hermite–Gaussian modes are indeed normal modes preserving their form through focus (Siegman 1986). To obtain an $N\times$ diffraction limit spot at focus the phase front of the incident laser beam was modified using a random phase plate with $N\times N$ cells across the beam. Whilst the actual phase fronts do not have this form the resulting amplitude and phase pattern at focus will not be too dissimilar to that of a typical $N\times$ diffraction limit spot (Biancalana and Chessa 1994). The results will represent the worst case situation for plasma wave generation. A typical intensity and phase front pattern near best focus for a $7\times$ diffraction limited spot is shown in figure 2. Note that the symmetry of the beam is the result of using only a small number of random phase plate cells across the beam and has been observed experimentally (Ceccotti *et al* 1995). It is clear from figure 2 that the beat wave is generated over a radial scale length of about one seventh of the spot size, the diffraction limit for the focusing lens. Thus, a more realistic value for the spot size in theoretical calculations is $\sigma = 25 \mu\text{m}$, although the beat wave in a real beam may well be generated over a larger radial dimension than this. The result is stronger ponderomotive blowoff limiting the plasma wave amplitude and lifetime below the values for the full spot size.

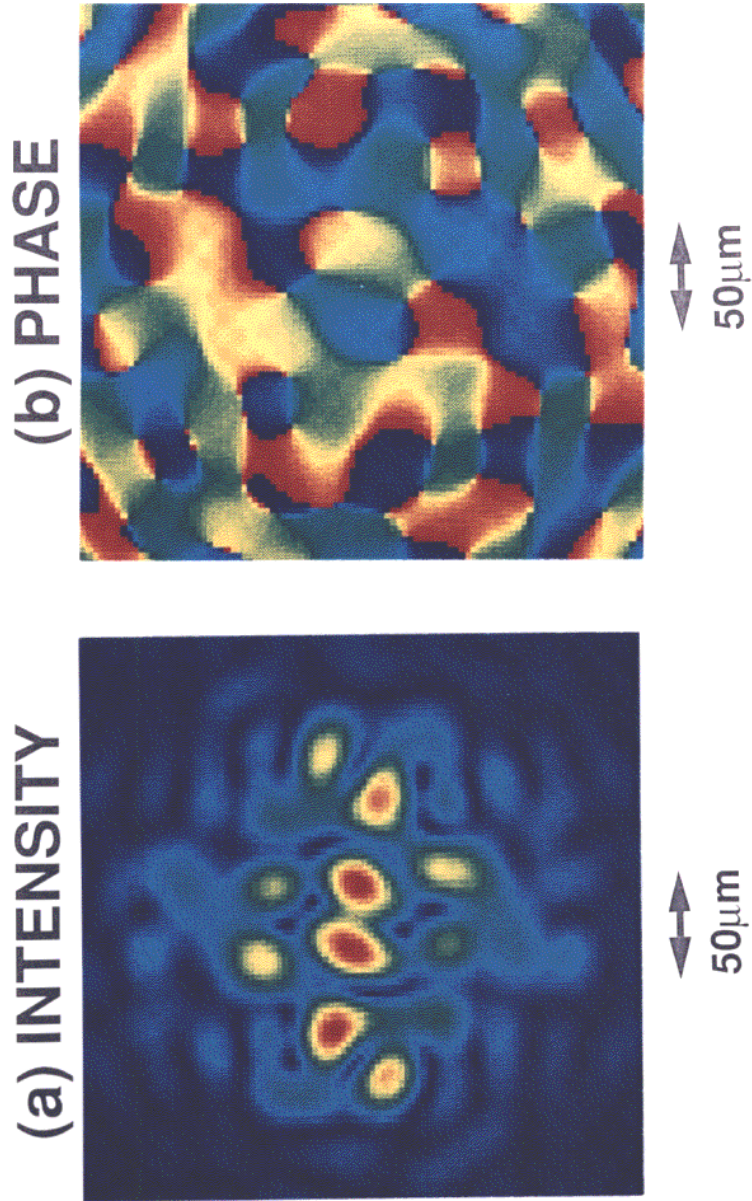


Figure 2. The calculated (a) intensity and (b) phase fronts at best focus for a $7\times$ diffraction limited spot.

3.3. The mixing box

The beams were combined under vacuum in a mixing box connected to the target chamber. A schematic illustration is presented in figure 3. The pump beams were orthogonally polarized so that a polarizer could be used to make the beams copropagating. Otherwise a 50:50 beamsplitter would be required resulting in the loss of half the energy. The multi-order waveplate gave full wave ($n\lambda$) delay at $1.064\ \mu\text{m}$ and half wave ($(n + 1/2)\lambda$) delay at $1.053\ \mu\text{m}$ so that both beams were horizontally polarized at output. The $F = 2\ \text{m}$, $f/20$ lens focused the pump beams into the centre of the target chamber. All the optical components were quartz and were mounted with motorized microdrives for alignment under vacuum.

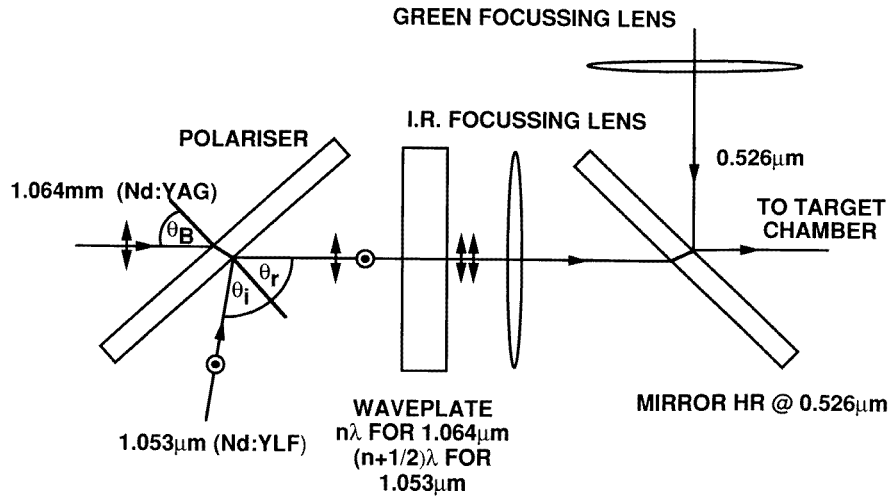


Figure 3. The mixing box for combining the two laser wavelengths under vacuum with minimum loss of energy.

The $0.526\ \mu\text{m}$ green probe beam was injected via a dielectric coated mirror transmitting at IR (see figure 3). Owing to dispersion a separate $F = 2\ \text{m}$, $f/20$ lens was needed to focus the green beam to the common focus of the IR pumps. Separate lenses also reduced the common path in quartz between the green and pump beams to reduce sideband generation by CARS in quartz. However, the coincidence of the beams in the optics was still sufficient to give unacceptably large sidebands. This coincidence was almost eliminated by placing 2 cm discs at the centre of each of the pump beams and using a corresponding 2 cm aperture stop on the green probe. This decreased the probe aperture to $f/100$ but reduced the sidebands to an acceptable level allowing detection of the plasma wave.

4. The experiment

4.1. Beam alignment and plasma formation

The experimental arrangement is shown in figure 4. The laser beams were fed into a spherical target chamber of 50 cm radius by a beam pipe. A glass microballoon of slightly smaller radius than the focal spot size was placed at the centre of the chamber to align the two IR pump beams and the green probe to a common focus. This was carried out

using low-power CW beams that followed the same path through the laser chain as the high-power beams. The microballoon was backlit by each beam and the image relayed onto a CCD camera using achromatic optics. The overall magnification of the system was a few thousand which permitted alignment to within $15 \mu\text{m}$. An equivalent plane monitor (EPM) was used to measure the spot size and verify the spatial coincidence of the beams in the focal plane on full power shots. The EPM consisted of an $F = 1 \text{ m}$ achromat with polaroid land film used to record the images. The measured spot radius corresponded to $\approx 7\times$ the diffraction limit.

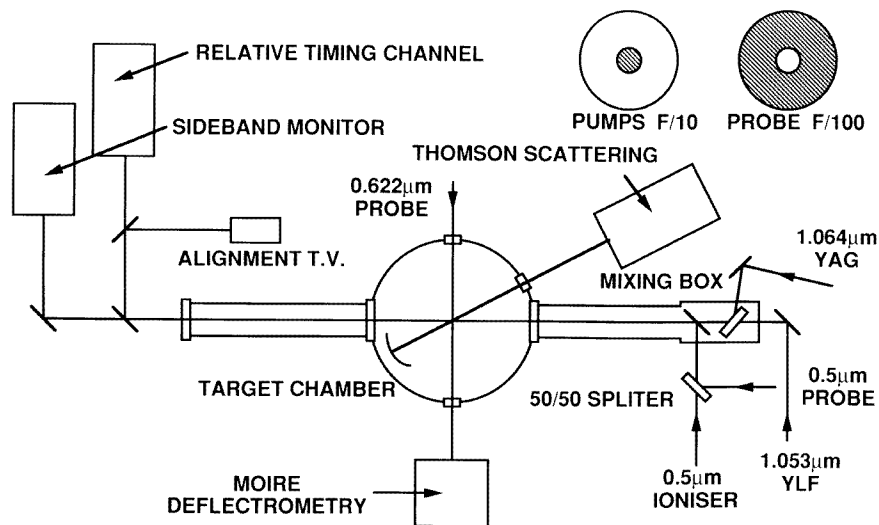


Figure 4. The beat wave experimental arrangement showing the positions of the diagnostic channels with respect to the target chamber.

The relative timing of all the beams at focus was checked for each shot using a spectrometer coupled to a Hadland Imacon 500 streak camera. The beams were dispersed in the spectrometer with the IR beams in first order and the frequency-doubled green beams in second order. This enabled verification of the timing of all the beams to within 20 ps.

The pump beams gave full ionization of the hydrogen fill gas in the focal region. Thus, the atomic density of the fill gas determined the resulting plasma electron density. The fill gas pressure and temperature were measured to within 1 mtorr and 0.1 K, respectively. This gave a 0.1% accuracy for the fill gas density at resonance. Full ionization of the fill gas was confirmed from Thomson scattering of the green probe. The scattered light was collected at the complementary angles of 20° and 160° . This was achieved using a spherical mirror to refocus the scattered light at 20° back into the focal spot so that this light then followed the light initially back scattered at 160° (see figure 4). The scattered light signals were collected by a spectrometer coupled to a Hadland Imacon 675 streak camera. The time dispersion of the streak camera enabled temporal resolution of the two spectra, the reflected signal arriving about 1 ns after the direct signal. These angles were chosen to give spectra with values of the scattering parameter $\alpha = 1/k\lambda_d$ of > 3 and < 0.5 for 20° and 160° , respectively. This enabled the plasma density and temperature to be separately determined (Evans and Katzenstein 1969). The pump beams gave a fully ionized plasma with a temperature of about 30 eV. The unapertured $0.526 \mu\text{m}$ probe also gave full

ionization with a plasma temperature of less than 10 eV.

To check that the beams were copropagating at focus the plasma columns produced by the beams were viewed transversely with a Moire deflectometry system (Kafri and Krasinski 1985). This is shown in figure 5(a) and used a low-energy Raman shifted probe at $0.632 \mu\text{m}$ which allowed wavelength discrimination from stray green light. The lenses placed before the Ronchi rulings gave a magnification of only about five. The diagnostic was run at this low magnification so that the length of the plasma produced could be measured. The rulings had a pitch $P = 50 \mu\text{m}$ (20 lines per mm) and a separation of $D \approx 70 \text{ cm}$. The beam deflection required to give one fringe shift is $\theta_1 \approx P/D \approx 0.1 \text{ mrad}$ and this sensitivity was just sufficient to detect the plasma. A set of relay lenses with an intermediate pinhole was used to eliminate the first-order diffraction image from the rulings which caused the image to be blurred. A deflectometry image for a full shot with the probe and pump beams is shown in figure 5(b). It was found that the ionization length on the beam axis was at least 5 mm. This should be compared with the Rayleigh length for the pump beams $z_r \approx 2F^2\lambda \approx 0.8 \text{ mm}$. Owing to the intentional low magnification the fringe shifts were not precise enough to allow the plasma density to be measured. However, in Dangor *et al* (1988) Thomson scattering shows that the plasma column generated is uniform to within a measurement accuracy of 4% over at least this length.

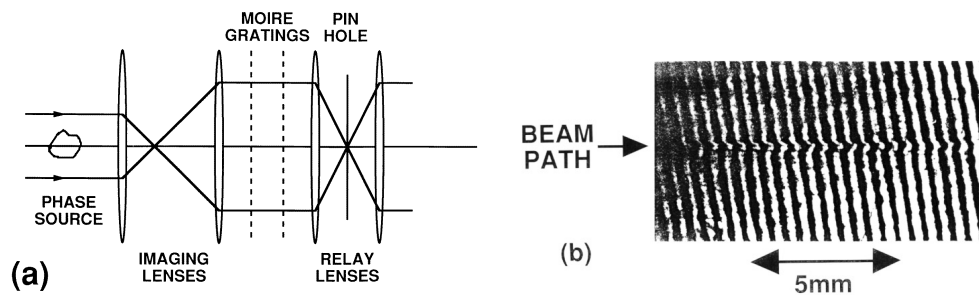


Figure 5. (a) Schematic of the Moire deflectometry channel. (b) Moire fringe image showing the copropagating plasma tracks of the pump beams and the probe beam for a typical shot.

4.2. Measurement of $\delta n/n$

The magnitude of the excited plasma wave was determined by measuring the relative amplitudes of the sidebands generated on the green probe by interaction with the plasma wave. These sidebands are of very low intensity and for this reason it was necessary to use a triple subtractive monochromator system. The pump beams were rejected before the first monochromator by 99% reflecting IR mirrors placed at the output of the target chamber. This eliminated any significant interaction between the pumps and $0.526 \mu\text{m}$ probe in the short air path to the first monochromator. The first monochromator dispersed the probe light, the central probe wavelength was then blocked and the remaining light recombined using the second monochromator. The third monochromator then redispersed the light and was set so that only the anti-Stokes spectrum was transmitted. This gave a sufficiently high rejection ratio to monitor the anti-Stokes sideband.

A streak record showing the anti-Stokes sideband formed on the $0.526 \mu\text{m}$ green probe with the plasma density tuned to resonance is shown in figure 6. A microdensitometer scan of this resonance data shot is given in figure 7. This shows the short lifetime of the sideband

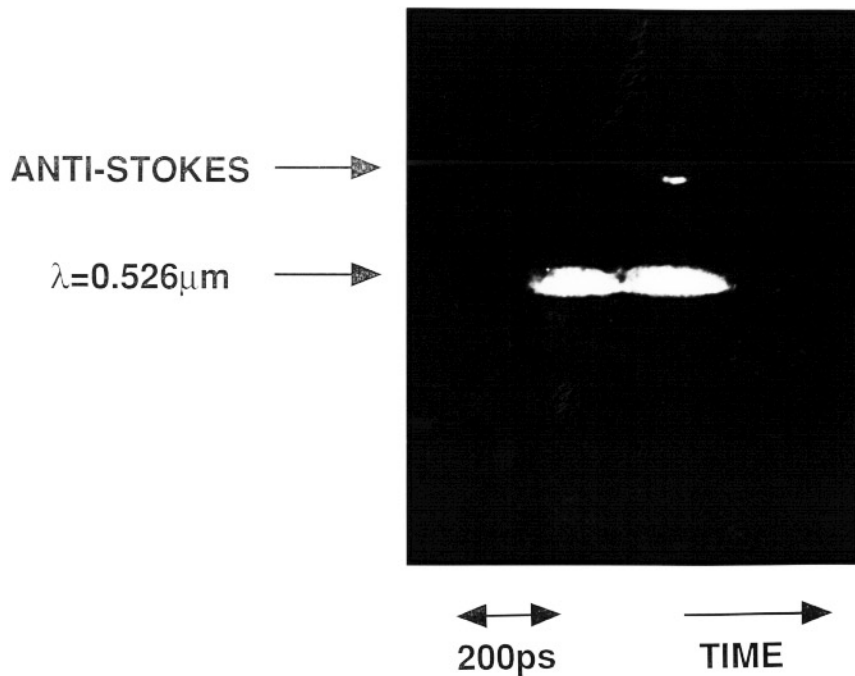


Figure 6. A streak camera record of the anti-Stokes sideband with the plasma density tuned to resonance.

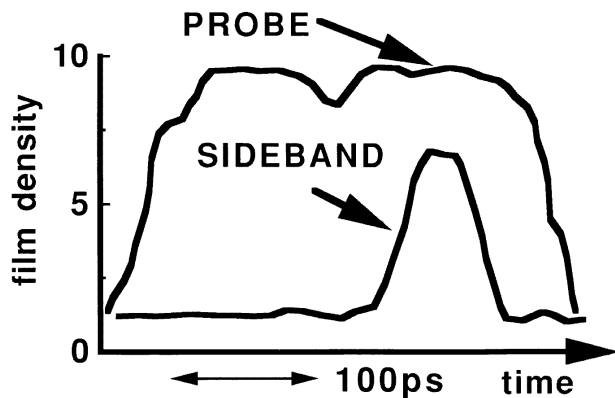


Figure 7. The microdensitometer scan of the resonance shot shown in figure 6. Notice the short lifetime of the sideband ≤ 50 ps indicating a short-lived plasma wave.

at ≤ 50 ps, the temporal resolution of the streak camera, indicating a short-lived plasma wave. The sideband amplitudes obtained for the pressure scan through the resonant density are presented in figure 8. An order of magnitude enhancement in the anti-Stokes signal was observed at resonance. This is taken as evidence of the generation of a beat wave. The small sideband levels on under resonance shots are due to residual CARS in the mixing optics. Data shots taken over resonance show an enhancement of about four times. This is

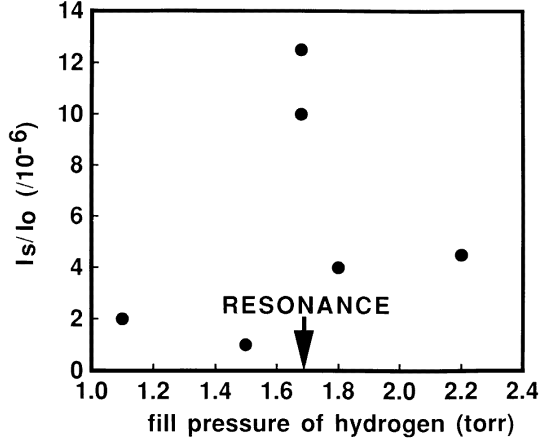


Figure 8. The sideband amplitudes on the green probe for the pressure scan through the resonant density. The order of magnitude enhancement at the resonance density is taken as evidence of a beat wave of $\delta n/n = 2\%$.

possibly due to the fact that some part of the plasma is always resonant for over-resonance fill pressures, due to incomplete ionization in the wings of the laser beams or expansion. This is clearly not possible for under-resonance fill pressures. The $f/100$ aperturing of the probe beam meant that it could only interact with plasma waves having $\beta \geq 0.5$ for ω , k matching.

The strength of the plasma wave is estimated from the relative sideband amplitude I_0/I_s using

$$\frac{I_s}{I_0} = \left[\frac{\pi L_{\text{eff}}}{2 \lambda_0} \left(\frac{\omega_p}{\omega_0} \right)^2 \frac{\delta n}{n} \right]^2. \quad (4.1)$$

The value at resonance is $I_s/I_0 \approx 1.3 \times 10^{-5}$. The length over which the plasma wave is generated is taken to be about 1–2 Rayleigh lengths where the pumps have highest intensity so that $L_{\text{eff}} \approx 0.8$ – 1.6 mm. This gives $\delta n/n \approx 0.8$ – 1.6% .

5. Comparison of results with theory and simulation

5.1. The envelope equation solution

We present here the theoretical evolution of the plasma wave allowing for an initial density mismatch from exact resonance and for ponderomotive blowoff which takes the system off resonance. We shall show that the experimental results are consistent with the plasma wave being generated over a radial dimension of the diffraction limit $\sigma \approx 25 \mu\text{m}$.

The growth and saturation of the plasma wave is modelled using the envelope approximation, in which the quickly varying phase $\exp(i(\omega_p t - k_p z))$ is removed (Karttunen and Salomaa 1986). We assume that the plasma wave is constant in the direction of propagation since the laser pulse length in our experiment is much longer than the length of the plasma ($c\tau_{\text{whm}}/l_{\text{plasma}} \approx 10$). The plasma wave amplitude $\delta n/n = \varepsilon$ is given by

$$\frac{\partial \varepsilon}{\partial t} = \frac{1}{4} \omega_p \alpha_0 \alpha_1 + i \frac{3}{16} \omega_p |\varepsilon|^2 \varepsilon - i \omega_p \delta \varepsilon - \frac{\nu \varepsilon}{2} \quad (5.1)$$

where

$$\alpha_i = \frac{eE_i}{m_e\omega_i c} \quad \delta = \frac{\omega_p - (\omega_1 - \omega_0)}{\omega_p} = \frac{1}{2} \frac{\Delta n}{n}. \quad (5.2)$$

The terms on the right-hand side of (5.1) represent, respectively, the axial ponderomotive force driving the plasma wave, relativistic detuning, linear detuning (or density mismatch) and a collisional damping term.

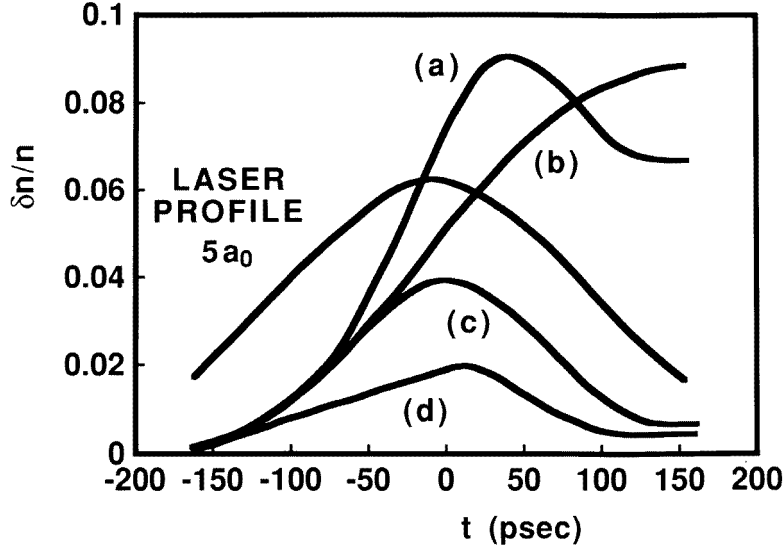


Figure 9. The plasma wave amplitudes $\delta n/n = \varepsilon$ for the density mismatches (a) $\Delta n/n = 0$, (b) $\Delta n/n = 0.25\%$, (c) $\Delta n/n = -0.25\%$ and (d) $\Delta n/n = 0.5\%$. The laser profile is also shown. The parabolic pulse length is related to the Gaussian fwhm by $t_p = 3/8 (\pi/\ln(2))^{1/2} \tau_{fwhm} \approx 0.8\tau_{fwhm}$.

We now consider the saturation amplitudes due to these competing effects, for our experimental conditions. We first neglect the collision term and ponderomotive blowoff to show the effect of varying the initial linear detuning term δ . This corresponds to not setting the initial density of the hydrogen fill gas to exact resonance. The results are presented in figure 9 where curves (a)–(d) show the plasma wave amplitudes for $\delta = 0, +0.125\%, -0.125\%, +0.25\%$ respectively. The density mismatch in each case is therefore $\Delta n/n = 0, +0.25\%, -0.25\%, +0.5\%$. The laser profile has $\alpha_0 = \alpha_1 = 0.01$ corresponding to $I\lambda^2 = 2 \times 10^{14} \text{ W cm}^{-2} \mu\text{m}^2$ and $\tau_{fwhm} = 200 \text{ ps}$. The results obtained should be compared with those for constant laser pumps (Rosenbluth and Liu 1972) for which $\delta n/n = (16\alpha_0\alpha_1/3)^{1/3} \approx 9\%$, in excellent agreement with curve (a) in figure 9. On the other hand curves (b), (c) and (d) of the same figure come under different detuning regimes. For curve (b) the density mismatch partly compensates for the relativistic detuning allowing the plasma wave to reach a higher amplitude than it does for $\Delta n/n \approx -0.25\%$ in curve (c). The ‘optimum’ value of $\Delta n/n$ for square pumps is 0.3% (Tang *et al* 1985). The maximum value in curve (d) is consistent with the ‘heavy detuning limit’ $(\delta n/n)_{\max} = \alpha_0\alpha_1(\Delta n/n)^{-1} \approx 2.8\%$ because our pulse length is slightly shorter than the time needed for the plasma wave amplitude to reach this value. Note that the above show the need to be within about 0.5% of exact resonance.

Although the temperature is rather low (≤ 30 eV, measured from Thomson scattering) the effective collision rate is considerably reduced by the electron quiver motion in the combined plasma wave and laser fields. An estimate of the saturation amplitude due to this modified collision frequency v_{eff} (Mora *et al* 1988) gives

$$(\delta n/n)_{\text{max}} \approx \frac{\alpha_0 \alpha_1 \omega_p}{2v_{\text{eff}}} \approx 5\%. \quad (5.3)$$

An additional and very significant density mismatch arises from the radial ponderomotive blowoff of ions from the centre of the laser beam (Mora *et al* 1988). Any ponderomotive blowoff axially can be neglected as the Rayleigh length is much longer than the spot size. We can include the ponderomotive blowoff in the envelope model by introducing a time-dependent mismatch term. The force on the ions due to the laser (in normalized units) is given by

$$\frac{m_i}{m_e} \frac{\partial v_i}{\partial t} = -\frac{\partial}{\partial r} \frac{\alpha_0^2 + \alpha_1^2}{4}. \quad (5.4)$$

We assume an intensity profile which is parabolic in time and Gaussian in the radial direction so that

$$\alpha_{0,1}^2 = \frac{a_{0,1}^2}{t_p^2} (2t t_p - t^2) \exp\left[-\frac{r^2}{\sigma^2}\right] \quad (5.5)$$

where $2t_p$ is the laser pulse rise time and σ the spot size. Here, $a_{0,1}$ are the quiver velocities on axis at the peak of each pump. On integrating (5.4) with the continuity equation we have for equal amplitude pumps

$$\frac{\partial n_i}{\partial t} = \frac{n_i a_0^2}{m_i \sigma^2 t_p^2} \left(\frac{t^3}{3} - t^2 t_p\right). \quad (5.6)$$

On integrating a second time we obtain the density mismatch

$$\frac{\Delta n}{n}(t) = \frac{m_e a_0^2}{3m_i \sigma^2 t_p^2} \left(\frac{t^4}{4} - t^3 t_p\right). \quad (5.7)$$

Assuming the plasma wave remains 'linear' and is not relativistically detuned i.e. $(\delta n/n) \propto \alpha_0 \alpha_1 t$ we can obtain an analogous expression for the density depletion due to the plasma wave ponderomotive force, again for parabolic pumps

$$\frac{\Delta n}{n}(t) = -\frac{m_e}{m_i} \frac{a_0^4}{16\sigma^2 t_p^4} \left(\frac{t^8}{504} - \frac{t^7 t_p}{63} + \frac{t^6 t_p^2}{30}\right). \quad (5.8)$$

Notice that over the pulse duration $0 \leq t \leq 2t_p$ the above equations give $\Delta n/n \leq 0$ corresponding to $\omega_p \leq \Delta\omega$, as they should.

The mismatch resulting from ponderomotive blowoff is shown in figure 10(a) for a laser spot and resulting plasma wave having radial dimension $\sigma = 25 \mu\text{m}$, $200 \mu\text{m}$. This corresponds to generating a plasma wave over the entire focal spot or over the diffraction limit of the focusing lens as suggested by the results of section 3. We notice that the plasma wave ponderomotive force dominates and the laser ponderomotive force can be neglected owing to an initial growth rate for the mismatch which is proportional to a_0^4 compared with a_0^2 . The plasma wave amplitudes corresponding to these mismatch curves are shown in figure 10(b). For $\sigma = 200 \mu\text{m}$ there is a mismatch of about 1% at the plasma wave maximum whose value of $\delta n/n \approx 6\%$ agrees rather well with the analytical estimate by Mora *et al* (1988) using only the plasma wave ponderomotive force. It is clear that $\sigma = 25 \mu\text{m}$ corresponds to our experimental results, suggesting that the plasma wave is generated over

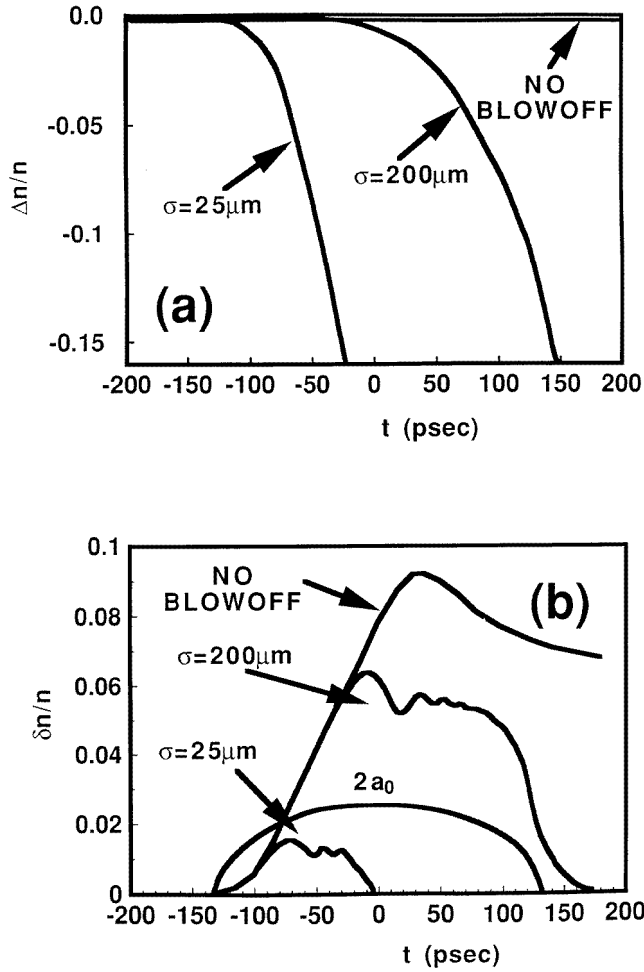


Figure 10. (a) The density mismatch $\Delta n/n$ due to ponderomotive blowoff for the laser parameters of our experiment and spot sizes of $\sigma = 25 \mu\text{m}$, $\sigma = 200 \mu\text{m}$. (b) The corresponding plasma wave amplitude $\delta n/n$ for the cases in (a).

this radial dimension. For this radius an increase in laser energy only results in the plasma wave reaching the same saturation amplitude earlier in the laser pulse. The rapid growth of the density mismatch also leads to a complicated rapidly damped wake, although we note that the mismatch expression (5.8) is invalid after the plasma wave saturates. Ideally, the mismatch should be integrated by including the plasma wave amplitude self-consistently. This would in general also cause the mismatch to saturate so that the curves in figure 10(a) are a 'worst case'.

In addition to the ponderomotive blowout a second possible limit on the plasma wave amplitude $\delta n/n$ due to the finite radial dimension of the laser beams is due to nonlinearities involving magnetic fields. These nonlinearities (Bell and Gibbon 1988) are important whenever the transverse structure is on the scale of the collisionless skin depth c/ω_p . For our experiment this requires the focal spot radius to be not smaller than $75 \mu\text{m}$ so we expect further reduction in plasma wave.

5.2. The modulational instability

It has been shown analytically that the plasma wave produced in long pulse (≥ 20 ps) beat wave experiments is subject to the modulational instability (Pesme *et al* 1988). Recent experiments by Amiranoff *et al* (1992) have confirmed this. For our experimental parameters the minimum growth time is about 10 ps when $\delta n/n \approx 2\%$, suggesting that this instability may be important. We have investigated this numerically using a 1D electrostatic PIC code to model one wavelength ($100 \mu\text{m}$) of the plasma wave. The wave is driven by an imposed sinusoidal longitudinal electric field moving at c and having the same wavelength as the plasma wave. This gives the ponderomotive force arising from the beating laser beams. The plasma was simulated with 20000 electrons and an equal number of protons with an initial temperature of 30 eV. The irradiance of each laser beam is taken to be $I = I_0 (1 - ((t - \tau)/\tau)^2)$ where $I_0 = 2.3 \times 10^{14} \text{ W cm}^{-2}$ and $\tau = 140$ ps (fwhm of 200 ps). Figure 11(a) is a plot against time of the amplitude of the Fourier component with wavelength $100 \mu\text{m}$. The plasma wave grows cleanly for the first 40 ps and then decays rapidly. The initially thin line on the graph thickens because the wave is no longer a travelling wave with constant amplitude but a partly standing wave with amplitude variation on a timescale of $1/\omega_p$. Once decayed the plasma wave recovers to reach a second peak at 100 ps. Thereafter, the wave decays again and the cycle is repeated at intervals of around 70 ps although the later cycles are less well defined. Figure 11(b) shows the rms deviation σ of the ion density from its mean (after smoothing over $1/2 \mu\text{m}$ to reduce statistical noise). As expected, growth in σ coincides with the plasma wave peaking and decaying with the

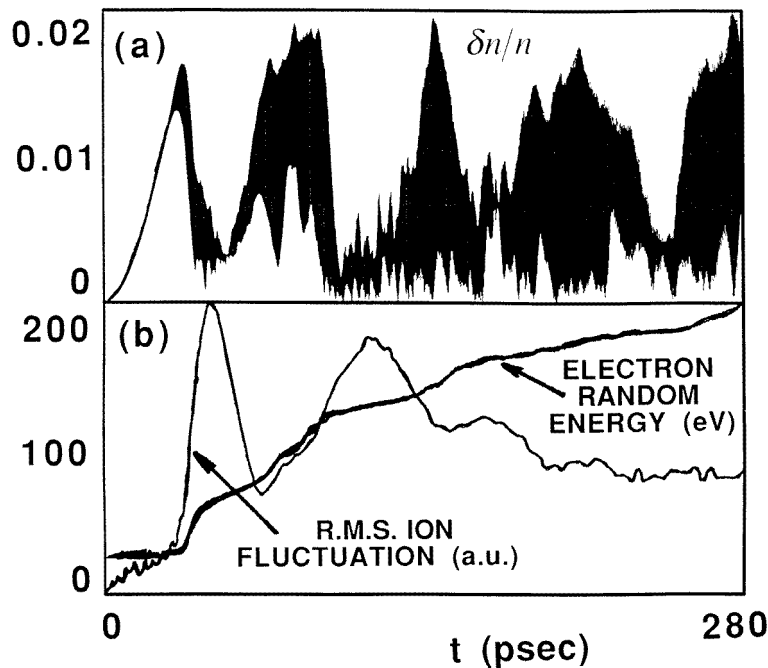


Figure 11. (a) The plasma wave amplitude $\delta n/n$ against time showing the limiting value of $\delta n/n$ due to the modulational instability. (b) the rms ion fluctuation and the electron random energy.

instability. During the periods when the plasma wave has small amplitude, σ reduces as the ion density relaxes. Also shown in figure 11(b) is the electron random energy, i.e. the electron energy after subtraction of the kinetic energy which is due to the plasma wave. This is a measure of the electron energy in thermal motion and non-resonant plasma waves. It shows that electrons gain thermal energy each time the plasma wave decays. The temperature increases with time and this affects the growth of the modulational instability since the wavelength for the maximum growth rate is proportional to the Debye length which increases as the temperature increases. This effect is seen in the simulation.

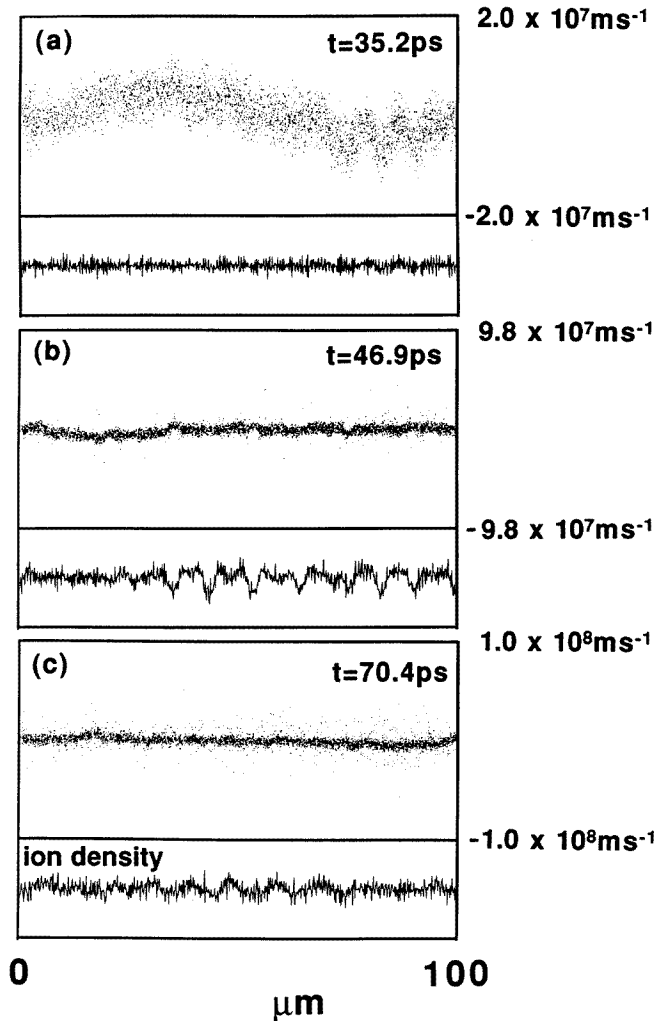


Figure 12. Plots of the electron distribution in phase space and the ion density at (a) 35 ps, (b) 47 ps and (c) 70 ps.

Figure 12 shows plots of the electron distribution in phase space and the ion density at three different times. After 35 ps the modulational instability is only just becoming noticeable. The electron distribution is essentially that expected for a 30 eV plasma supporting a plasma wave and the ion density is nearly uniform except for statistical noise.

However, the electron distribution shows signs of short wavelength structure near the right-hand end of the grid and the ion cavities are beginning to form. After 47 ps the modulational instability has caused the plasma wave to decay. The wave energy has been given to a suprathermal population of electrons (note the change of scale in the velocity ordinate) and the mean electron energy has increased by a factor of about two. The ion density distribution is heavily modulated on a scale length which is consistent with the expected wavelength of $\approx 8 \mu\text{m}$ for maximum growth of the instability (Pesme *et al* 1988). Once the plasma wave has collapsed the ion distribution begins to relax towards uniformity. The ion acoustic transit time across $8 \mu\text{m}$ is 75 ps (although ion acoustic waves are heavily damped in this case) so by 70 ps we see that the ion density is more uniform than at 47 ps. Once the ion density has relaxed the electron plasma wave grows again only for the instability to reoccur and the cycle is repeated.

The simulation clearly shows all the hallmarks of the modulational instability and leads us to expect it to occur in our experiment. The maximum wave amplitude in the simulation is 2%, which agrees very well with the experimental measurement and is the expected value given in Mora *et al* (1988). Experimentally, no evidence is seen for the periodic growth and decay of the plasma wave but this discrepancy with simulation may possibly be due to variation in intensity across the laser beam thus causing the peaks and troughs to occur at different times or ponderomotive blowoff at later times.

6. Conclusions and discussion

We have observed a relativistic plasma wave of amplitude $\delta n/n \approx 2\%$ and lifetime ≤ 50 ps induced by the beating together of two neodymium glass laser beams at $1.064 \mu\text{m}$ and $1.053 \mu\text{m}$. This required a plasma homogeneous to within 0.5% of resonant density. A suitable plasma has been shown to be generated by multiphoton ionization of the hydrogen fill gas by the two IR pump beams. The plasma wave had to be detected by a separate $0.526 \mu\text{m}$ probe to avoid SRS in the atmosphere and CARS in the common optics that would otherwise make observation of the plasma wave impossible. For our experimental conditions the maximum plasma wave amplitude and lifetime due to relativistic detuning are $\delta n/n \approx 8\%$, $\tau_p \approx 200$ ps, much larger than our observed values. A diffraction code for our $\approx 7\times$ diffraction limited spot shows that the plasma wave is driven over a radial dimension of the diffraction limit. We have shown numerically that the resulting ponderomotive blowoff, due mainly to the plasma wave electric field, drives the plasma density off resonance and so limits the maximum amplitude and lifetime of the plasma wave to our observed values. For this radial dimension, increasing the pump intensity only results in the plasma wave reaching the same saturation value earlier in the pulse. In addition, we have shown numerically that the modulational instability alone would also limit the plasma wave amplitude and lifetime to our observed values.

Acceleration of injected electrons using CO_2 laser beams giving $\delta n/n > 10\%$ (Clayton *et al* 1993, Ebrahim 1994) and using neodymium laser beams giving $\delta n/n \approx 2\%$ (Amiranoff *et al* 1995) shows that the beat wave process does work as a possible accelerator scheme. The most important parameters for beat wave experiments are the growth rate of the plasma wave $\propto \alpha_0 \alpha_1 \propto I \lambda^2$ compared with that of the modulational instability, the ponderomotive force due to the plasma wave $\propto 1/\sigma$ and the maximum allowable density mismatch $\Delta n/n \propto I \lambda^2$. The larger $I \lambda^2 (\geq 10^{16} \text{ W cm}^{-2} \mu\text{m}^2)$ in CO_2 experiments allows the plasma wave amplitude to grow too quickly to be limited by the modulational instability (Mora *et al* 1988). Also, ponderomotive blowoff is much less of a problem in CO_2 experiments because of the larger diffraction limited spots $\sigma \propto \lambda$ and the larger allowable density mismatch $\Delta n/n$ (Karttunen

1989). For these reasons CO₂ experiments obtain much larger plasma wave amplitudes. In order to obtain similarly large amplitudes using neodymium lasers, it is necessary to use much larger intensities to obtain the same $I\lambda^2$. Our scaling results show that for the necessary $I\lambda^2 \geq 10^{16} \text{ W cm}^{-2} \mu\text{m}^2$ the pumps have $\omega_p\tau \approx 200$, i.e. $\tau \leq 10 \text{ ps}$, with energy $W_{\text{laser}} \geq 30 \text{ J}$ and so allowing a density mismatch of $\Delta n/n \geq 2\%$. At these intensities relativistic self-focusing may allow the generation of plasma waves over distances greater than the Rayleigh length of the pump beams (Gibbon 1990). A possible future experiment is the use of close to diffraction limited pump beams focused to $\sigma \approx \lambda_p$ with pulse lengths $\leq 10 \text{ ps}$ and 100 ps to give rapid plasma wave growth while still allowing relatively easy beam synchronization. In such an experiment the ion waves of the modulational instability could be monitored directly by Thomson scattering.

References

- Amiranoff F *et al* 1992 *Phys. Rev. Lett.* **68** 3710
 Amiranoff F *et al* 1995 *Phys. Rev. Lett.* **74** 5220
 Bell A R and Gibbon P 1988 *Plasma Phys. Control. Fusion* **30** 1319
 Biancalana V and Chessa P 1994 *Appl. Opt.* **33** 3465
 Ceccotti T, Bastiani S, Giulietti A, Giulietti D and Danson C 1995 *Inst. Phys. Conf. Ser. No. 140* Section 9
 Clayton C E *et al* 1985 *Phys. Rev. Lett.* **54** 2343
 Clayton C E *et al* 1993 *Phys. Rev. Lett.* **70** 37
 Cohen B I, Kaufman A N and Watson K M 1972 *Phys. Rev. Lett.* **29** 581
 Cohen B I, Cohen R H, Logan B G, Nevins W M, Smith G R, Kluge A V and Kritiz A H 1988 *Nucl. Fusion* **28** 1519
 Dangor A E, Dymoke-Bradshaw A K L and Dyson A 1988 *J. Appl. Phys.* **64** 6182
 ———1990 *Phys. Scr.* T **30** 107
 Dangor A E *et al* 1989 *J. Phys. B: At. Mol. Opt. Phys.* **22** 797
 Danson C N 1990 *MPhil Thesis* Newcastle upon Tyne Polytechnic, and Rutherford Appleton Laboratory Report RAL-90-011
 Dyson A *et al* 1989 *J. Phys. B: At. Mol. Opt. Phys.* **22** L231
 Ebrahim N A 1994 *J. Appl. Phys.* **76** 7645
 Ebrahim N A *et al* 1986 *IEEE Trans. Nucl. Sci.* **32** 3539
 Evans D E and Katzenstein J 1969 *Rep. Prog. Phys.* **32** 207
 Gibbon P 1990 *Phys. Fluids B* **2** 2196
 Kafri O and Krasinski J 1985 *Appl. Opt.* **24** 2746
 Karttunen S J and Salomaa R R E 1986 *Phys. Rev. Lett.* **29** 701
 ———1987 *IEEE Trans. Plasma Sci.* **PS-15** 134
 ———1989 *Phys. Scr.* **39** 741
 Karttunen S J, Pattikangas T J H, Salomaa R R E and Sipila S K 1991 *Nucl. Fusion* **31** 1079
 Keldysh L V 1965 *Sov. Phys.-JETP* **20** 1307
 Kitagawa Y *et al* 1992 *Phys. Rev. Lett.* **68** 48
 Kuizenga D and Siegman A 1970 *IEEE J. QE* **6** 694
 Leemans W P *et al* 1992 *Phys. Rev. A* **46** 1091
 Marques J R *et al* 1993 *Phys. Fluids B* **5** 597
 Mora P, Pesme D, Heron A, Laval G and Silvestre N 1988 *Phys. Rev. Lett.* **61** 1611
 Pesme D, Karttunen S J, Salomaa R R E, Laval G and Silvestre N 1988 *Laser and Particle Beams* **6** 199
 Rogers J H, Hwang D Q, Thomas J C, Horton R L, Killeen J and Dimonte G 1992 *Phys. Fluids B* **4** 1920
 Rosenbluth M N and Liu C S 1972 *Phys. Rev. Lett.* **29** 701
 Siegman A 1986 *Lasers* (Mill Valley, CA: University Science Books)
 Tajima T and Dawson J M 1979 *Phys. Rev. Lett.* **43** 267
 Tang C M *et al* 1985 *Phys. Fluids* **28** 1974